Materials Research Express

Synthesis and characterization of liposomes encapsulating silver nanoprisms obtained by millifluidic-based production for drug delivery

To cite this article before publication: Fatih Yanar *et al* 2023 *Mater. Res. Express* in press https://doi.org/10.1088/2053-1591/acf192

IOP Publishing Journal Title
Journal **XX** (XXXX) XXXXXX https://doi.org/XXXX/XXXX

Synthesis and characterization of liposomes encapsulating silver nanoprisms obtained by millifluidic-based production for drug delivery

Fatih Yanar [1, 2,*], Harriet Kimpton [2], Domenico Andrea Cristaldi [2], Ali Mosayyebi [2, 4], Dario Carugo [3], Xunli Zhang [2,*]

[1] Department of Molecular Biology and Genetics, Bogazici University, Istanbul, Turkey
[2] Department of Mechanical Engineering, Faculty of Engineering and Physical Sciences, University of Southampton, Southampton SO17 1BJ, UK
[3] Nuffield Department of Orthopaedics, Rheumatology and Musculoskeletal Sciences (NDORMS), University of Oxford, Oxford OX3 7LD, UK
[4] Institute for Life Sciences (IfLS), University of Southampton, Southampton SO17 1BJ, United Kingdom
[*] Corresponding authors: fatih.yanar@boun.edu.tr; XL.Zhang@soton.ac.uk

Abstract

Silver nanoprisms (SNPs) have attracted significant attention due to their surface plasmon resonance behaviour, which is strongly dependent on their size and shape. The enhanced light absorption and scattering capacity of SNPs, make them a promising candidate system for non-invasive imaging and drug delivery in nanoparticle-assisted diagnostics and therapy. However, systemic administration of silver nanoparticles (AgNPs) at high concentrations may result in toxic side-effects, arising from non-targeted bio-distribution. These drawbacks could be mitigated by employing liposomes as carriers for AgNPs. However, there is a lack of systematic studies on production and subsequent physico-chemical characterisation of liposomal systems encapsulating SNPs. The present study therefore investigated the synthesis of liposomes encapsulating SNPs (Lipo/SNPs) using a continuous-flow millimetre-scale reactor, whereby liposome formation was governed by a solvent exchange mechanism. An aqueous phase and an ethanolic lipid phase were conveyed through two separate inlet channels, and subsequently travelled through a serpentine-shaped channel where mixing between the two phases took place. The synthesis process was optimised by varying both liposome formulation and the operating fluidic parameters, including the ratio between inlet flow rates (or flow rate ratio) and the total flow rate. The obtained Lipo/SNPs were characterised for their size and electrostatic charge, using a dynamic light scattering apparatus. Liposome morphology and encapsulation efficiency of SNPs within liposomes were determined by transmission electron microscopy (TEM) imaging. The synthesised negatively charged Lipo/SNP samples were found to have an average size of ~150 nm (size dispersity < 0.3). The AgNPs encapsulation efficiency was equal to 77.48%, with mostly single SNPs encapsulated in liposomes. By using a multiangle TEM imaging approach, quasi-3D images were obtained, further confirming the encapsulation of nanoparticles within liposomes. Overall, the formulation and production technique developed in the present study has potential to contribute towards mitigating challenges associated with AgNP-mediated drug delivery and diagnostics.

Keywords: silver nanoparticles, silver nanoprisms, liposomes, encapsulation, millifluidics, dynamic light scattering, transmission electron microscopy

1. Introduction

Silver nanoparticles (AgNPs) are of significant interest in numerous fields of science because of their antimicrobial, optical, and thermal properties [1]. These characteristics of AgNPs have paved the way for their usage in several areas of application, including electrochemistry, catalysis, food and pharmaceuticals, and nanomedicine [2]. In biomedical applications, AgNPs have been widely used as imaging probes and plasmonic antennas due to their unique optical properties [3–5].

There are different shapes of AgNPs such as spherical, rod-like, triangular, or hexagonal [6], which can be tuned according to the method of particle synthesis. Particle shape and size play an important role on its surface plasmon resonance (SPR) behavior, which can in turn dramatically influence its physical properties and overall performance, e.g. including antimicrobial and optical characteristics [7]. For instance, the absorption wavelength of AgNPs can be tuned across visible and near-infrared (NIR) light. Owing to these properties, AgNPs with different shape and size have great potential in light-controlled drug delivery systems and for real-time detection of cancerous tissue [8].

Among different shapes of AgNPs, silver nanoprisms (SNPs) exhibit remarkable optical features, largely due to their SPR behavior arising from their sharp tip morphology and height/length/thickness ratio [9], resulting in greater light absorption and scattering capacity when compared to spherical nanospheres (SNS) [10–12]. As a result, SNPs have been applied in a broad range of areas, including solar cells, catalysis, and biomedicine [13–16]. Moreover, SNPs hold great potential as tools to achieve simultaneous diagnostic and therapeutic functions, often referred to as 'theranostics'. However, bio-distribution of AgNPs at high concentrations may result in systemic toxicity arising from non-targeted delivery [17].

Studies investigating the toxicity profile of AgNPs have revealed their cytotoxic effects, through the generation of reactive oxygen species (ROS) or the alteration of gene expression, ultimately resulting in cell death. Proposed cytotoxic mechanisms include the interaction of AgNPs with cell membranes, leading to ROS generation and apoptosis [18]. It has also been suggested that the adhesion of AgNPs to cell membranes could cause structural damage, leading to leakage of intracellular compounds and subsequent cell death [19]. Additionally, the release of Ag^+ ions from AgNPs can impact intracellular O_2 levels and also trigger ROS generation [20]. Studies investigating the effect of AgNPs as anticancer agents, demonstrated their ability to induce ROS generation and affect the regulation of cell division and expression of regulatory genes such as cyclin B1 [21]. AgNPs have also exhibited cytotoxic action against HeLa and B16 melanoma cells [22]. It is also worth mentioning that the cytotoxic effects of AgNPs can vary depending on their size and shape. It has been previously demonstrated that when the size of AgNPs is reduced from 45.5 nm to 22.4 nm, it could result in greater toxicity in bovine retinal endothelial cells [23]. It has also been shown that silver wires (100 nm in diameter) have a detrimental effect on alveolar epithelial cell viability, whilst the effect of silver nanospheres (SNSs) is insignificant [24]. Although these earlier findings show the potential of AgNPs as anticancer agents, particle accumulation in healthy tissues can lead to undesired systemic toxicity. This also poses a limit to the concentration of AgNPs that can be safely administered for therapeutic purposes. The encapsulation of AgNPs within a carrier system may provide an efficient route to potentially reduce their systemic toxicity. In efforts to achieve localized delivery of AgNPs while minimizing toxic side-effects, previous *in vitro* studies have demonstrated that delivery of AgNPs within liposomes was associated with greater therapeutically favourable effects at lower concentrations, when compared to the delivery of unencapsulated AgNPs alone [25,26]. These earlier findings thus suggest that encapsulation of SNPs in liposomes offers a promising route for reducing

off-target systemic effects, as well as providing a potential platform for co-delivery of AgNPs together with active pharmaceutical ingredients to achieve controlled and localized drug delivery.

Liposomes are vesicular systems composed of natural or synthetic lipids (mainly phosphatidylcholines) and consist of a lipid bilayer shell encapsulating an aqueous compartment. It has been evidenced that liposomes have characteristics of high biocompatibility and biodegradability, increased biologic half-life, as well as the ability to be loaded with both hydrophilic and hydrophobic molecules [27–29]. Liposomal formulations have proven to be effective in delivering a range of bioactive agents to specific sites within the body, while minimizing toxic side-effects of these agents on healthy tissues [30–32]. These features thus make liposomes an attractive vehicle for the delivery of anticancer and many other classes of compounds, including particulate systems like SNPs. Scalable and controllable production of particle-encapsulating liposomes however remains a challenge, and only limited work has been carried out in this area of research [33,34]. Although methods relying on continuous-flow reactors have been previously employed for producing either liposomes or AgNPs, their application to the production of SNP-encapsulating liposomes is largely unexplored. To the best of the authors' knowledge, no previous study has specifically reported on a systematic physico-chemical characterization of SNPs encapsulation within liposomes produced using a continuous-flow reactor.

The present study therefore aimed to develop a method to produce liposomes encapsulating SNPs based on a millimetre-scale flow reactor (or 'millireactor'), and to characterize the properties and encapsulation efficiency (*EE*%) of the produced liposomes using dynamic light scattering (DLS) and transmission electron microscopy (TEM) techniques (including a multi-angle quasi-3D TEM imaging approach). Results from the present study demonstrate the applicability of continuous-flow reactors as a technology platform for producing SNP-encapsulating liposomes, and contribute towards our understanding of the physico-chemical properties of particle-encapsulating liposomal systems for potential application in theranostics.

Moreover, these findings provide a contribution towards the identification of suitable production techniques that can potentially facilitate future translation of SNP-based formulations with reduced systemic toxicity and potential for stimuli-mediated and controlled drug delivery.

2. Methods and Materials

2.1 Materials

PHOSPHOLIPON®90G (phosphatidylcholine, PC) was obtained from Phospholipid GmbH (Lipoid, Germany). Ethanol (99%), cholesterol (Chol, 99%), silver nitrate ($AgNO_3$, 99%), tri-sodium citrate dihydrate (TSCD), polyvinylpyrrolidone (PVP, average molecular weight AMw ≈ 29,000 $gmol^{-1}$), hydrogen peroxide (H_2O_2, 30% by weight (wt-%)), and sodium borohydride ($NaBH_4$, 99%) were obtained from Sigma Aldrich (Gillingham, UK). All water employed in the study was Milli-Q.

For delivering reagents into the millifluidic reactor, the following materials and instruments were employed: syringe pumps (AL-1010) from World Precision Instruments (Hertfordshire, UK); 20 mL BD-Plastipak syringes with Luer lock connectors from Fisher Scientific (Loughborough, UK); polytetrafluoroethylene (PTFE) tubing, male Luer lock rings, and a hot plate stirrer (UC152D) from Cole-Parmer (St. Neots, UK). The outlet port of the millireactor was connected to a collection vial using a 21.5 cm long PTFE tubing. The inner and outer diameter of the tubing were 0.5 mm and 1.6 mm, respectively. The connection between syringes and inlets of the reactor was made using PTFE tubing.

2.2 Millifluidic reactor for the synthesis of liposomal systems

PC and Chol were dissolved in ethanol at different concentrations to prepare stock solutions to be used in liposome synthesis. In continuous-flow liposome production by solvent exchange mechanism using the millireactor, the ethanolic lipid solution and aqueous phase (water) were injected through the two inlet channels of the millireactor. The resultant dispersion was collected from the outlet into a vial. The architecture of the millireactor includes a 60 mm long serpentine mixing channel (radius of curvature: 1.15 mm) having a square cross-section (1 mm × 1 mm). The millireactor has two inlets (width: 0.40 mm, height: 1 mm) separated by a 0.2 mm wide septum, and one outlet. The fabrication of the device was performed using a previously published protocol that combined micromilling with replica moulding techniques [35–37]. A schematic of the device, including key dimensional characteristics, is shown in Figure 1.

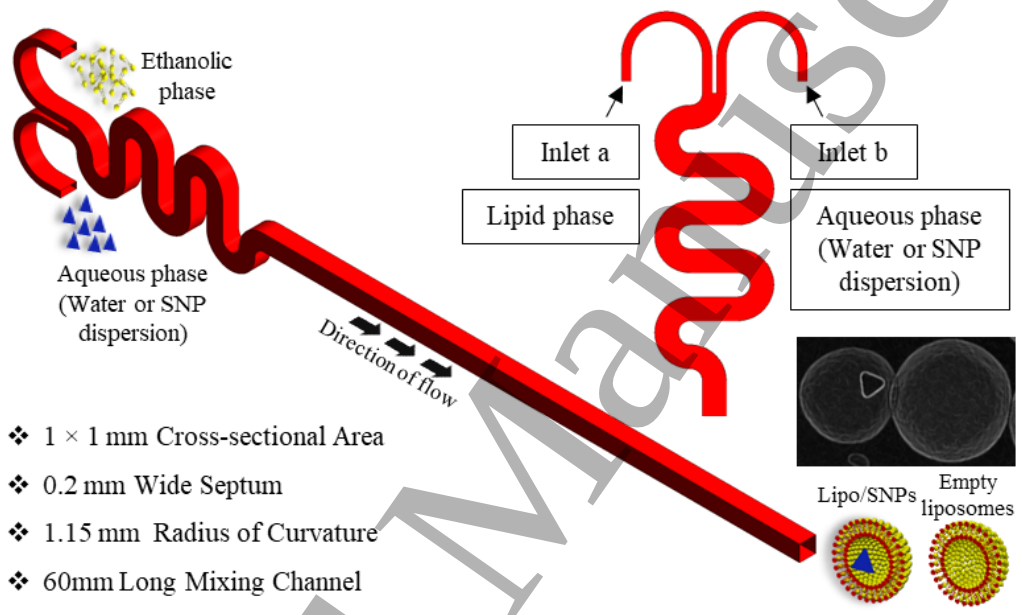

Figure 1. Schematic illustration of the experimental system employed for the production of empty liposomes and Lipo/SNPs using the millireactor. Lipo/SNPs: liposomal dispersions encapsulating SNPs; SNPs: silver nanoprisms.

2.3 Synthesis of SNPs

For the batch synthesis of SNPs, 24 mL of a solution containing TSCD (0.1 M, 0.375 mL), $AgNO_3$ (0.05 M, 0.05 mL), PVP (0.7 mM, 0.375 mL), and H_2O_2 (30 wt.%, 0.125 mL) was stirred vigorously at room temperature. After 7 minutes, a freshly prepared solution of $NaBH_4$ (25 mM, 1 mL) was rapidly injected. After about 30 minutes, the solution's colour changed from yellow to orange-brown, then to green-blue through to blue after a further 5 - 10 minutes. Stirring was subsequently stopped, and the resultant SNP dispersion was stored in the dark at 4 °C.

2.4 Synthesis of Lipo/SNPs

Continuous-flow synthesis of liposomes encapsulating SNPs (herein referred to as Lipo/SNPs) was performed using a similar protocol to the one employed for liposome production. Briefly, the ethanolic phase (including lipids) and the aqueous phase (SNP dispersion) were injected through the two inlets of

the millireactor, and the resultant dispersion was collected from the outlet in a vial as illustrated in Figure 1.

The experiments were conducted under different fluidic conditions, corresponding to variations in both flow rate ratio (FRR) and total flow rate (TFR). FRR is herein defined as the ratio between the volumetric inlet flow rate of the aqueous phase over the flow rate of the ethanolic lipid solution, while TFR is the total volumetric flow rate (i.e., the sum of flow rates imposed at the device inlets). The experimental conditions, including flow parameters and formulation characteristics, for each liposomal dispersion are summarised in Table 1.

Table 1 The fluidic operational parameters and chemical formulation of the produced liposomal dispersions.

Batch code [a]	Sample	Flow parameters	Lipid composition (mM) [b]	
		TFR (mL/min) / FRR	PC	Chol
#1	Liposome	1 / 10	11.2	4.8
#2	Lipo/SNP	5 / 10	28	12
#3	Lipo/SNP	1 / 25	100	-
#4 [c]	Liposome and Lipo/SNP	1 / 10	16	-

[a] The batch code given identifies a produced liposome or Lipo/SNP sample, with its corresponding flow parameters and chemical formulation. [b] Values indicate phospholipid (phosphatidylcholine soybean (P90G)) or stabilizer (cholesterol (Chol)) content of liposome or Lipo/SNP samples; values are given in millimolar (mM) concentration. [c] In the sample production, HEPES was used (20 mM, pH 7.4) in the aqueous phase as the buffer solution.

2.5 Characterization of liposomal dispersions

2.5.1 Size, size dispersity and zeta potential measurements

The geometrical properties and electrostatic charge (i.e., measured as zeta potential) of the liposomal dispersions were characterized by DLS technique, using a Zetasizer Nano ZS (Malvern Instruments Ltd., Malvern, UK). The measurements were performed at 25 °C, using folded capillary cell (DTS1070, Malvern Instruments Ltd., Malvern, UK) type cuvettes. Zetasizer Software 7.12 was used to determine the liquid viscosity of the samples analysed, by considering the effects of the different FRR values employed in the experiments [38].

Evaluations of liposome size and size distribution were carried out by considering the intensity-based distributions from DLS, as recommended in ISO 13321 and ISO 22412 [39,40]. However, number- and/or volume-based distributions were given as additional plots when needed, to obtain further insights on the dimensional properties of the dispersions.

The refractive index (RI) of the material is not taken into consideration in the calculation of intensity-based distributions, while it is used to determine the volume and number-based distributions. This is important for dispersions including more than one type of nanomaterial (i.e., for Lipo/SNP samples), as the conversion of intensity-based distributions to number or volume-based distributions may lead to inaccurate results. Here, the lipid RI value was chosen for the characterization of Lipo/SNPs due to difficulties in the estimation of the actual RI for the mixture of liposomes and SNPs. Also, in this technique, the conversion from intensity to volume- or number-based distributions assumes that the dispersion is homogenous and that all of the nanoparticles are spherical. In this study, the Lipo/SNPs were not fully spherical likely due to the anisotropic shape of SNPs and the dispersion was not homogeneous due to possible inter-particle aggregation. Based on these reasons, the use of intensity-based distributions rather than number and volume-based distributions was found more reliable [39].

It is also important to note that the data used in the size distribution plots were obtained by selecting the "*multiple narrow modes (high resolution)*" option in the Zetasizer software. This mode is recommended for samples that can contain discrete particle size populations [39,41]. Notably, the selection of this measurement mode resulted in multiple peaks in the size distribution plots, indicating the presence of multiple populations in the sample, while the "*general purpose (normal resolution)*" mode generally showed only one peak in the size distribution plots.

2.5.2 Image analysis of Lipo-SNPs

TEM was used to image the liposomal dispersions. The experimental procedure was performed by placing a 5 µL sample volume (of liposomes or Lipo/SNPs) on a carbon-coated grid and left for adsorption for 30 s. A filter paper (Whatman) was used to remove any excess liquid. Then, the negative stain technique was employed on the grid by adding 5 µL of 5% ammonium molybdate containing 1% trehalose (for 30 s). By using a filter paper, any further sample excess was removed. A Tecnai T12 microscope (FEI, Hillsboro, OR, USA) was employed to capture TEM images. SNP samples were characterized following the same protocol but without performing the negative staining step. The *EE*% of SNPs in liposomes was also calculated from TEM images by manual particle counting, using Equation 1 below.

$$\frac{\textbf{Total number of SNPs in the image} - \textbf{number of free SNPs in the image}}{\textbf{Total number of SNPs in the image}} \boldsymbol{x\ 100} \qquad \textbf{(1)}$$

2.5.3 Image analysis of resin-embedded Lipo/SNP samples

The Lipo/SNP samples were also characterized with an additional TEM-based process, in order to gain additional evidence of SNPs encapsulation. This process involved embedding Lipo/SNP samples into a resin, which was subsequently sliced into thin sections.

Briefly, 1 mL of Lipo/SNP sample was mixed with the fixative glutaraldehyde (2.5% concentration) and incubated for 1 hour. Subsequently, the sample was embedded in alginate for 20 minutes and rinsed twice with water for 10 minutes. Then, the sample was mixed with osmium tetroxide (1% concentration) as a post-fixative, and incubated for 1 hour. The sample was rinsed again, and uranyl acetate (2.5% concentration) was added. After 20 minutes, the sample was rinsed five times with ethanol for 10 minutes, at increasing ethanol concentration (at 30%, 50%, 70%, 95%, and 100%) each time. Then, a 50:50 acetonitrile:resin mixture was added to the sample and incubated overnight. Finally, the sample was embedded in fresh resin, which was polymerized at 60 °C for 24 hours. The obtained embedded sample of liposomes was sliced using an ultramicrotome to obtain very thin slices with a thickness of approximately 800-900 Å. Slices were then placed on a carbon-coated grid and imaged using the TEM microscope.

TEM images of the same section were taken at different angles (+30° to -30°) to obtain a quasi-3D image so that the location of nanoparticles could be assessed and characterized more effectively.

3. Results and Discussion

3.1 Continuous-flow synthesis of liposomes encapsulating SNPs

In the continuous-flow synthesis of liposomes by solvent exchange mechanism, the formation of lipid vesicles is typically driven by the increase in polarity at the interface between an aqueous phase and an organic phase (such as ethanol) in which lipids are solubilised. Due to their amphipathic nature, lipid

molecules spontaneously self-assemble into vesicular structures (typically in milliseconds) upon increase in the polarity of the surrounding medium [42]. The ratio of the aqueous and ethanolic volumetric flows, the concentration of lipids, and the mixing regime are key factors in affecting this process [35]. Depending on the architecture of a flow reactor, the formation of vesicles can be dominated by diffusion-based mixing (e.g., in devices with cross-flow geometry) [43] or advection-based mixing (e.g., in devices with serpentine or spiral shaped microchannels) [44]. As for the production of loaded liposomes, the payload can be injected within either the aqueous or the organic phase depending on its solubility in these media, and the encapsulation process typically takes place during the vesicle self-assembly. The payload may therefore localise within the aqueous core of the vesicle or in the lipid bilayer depending on its affinity for hydrophilic or lipophilic environments.

In the millifluidic-based production of Lipo/SNPs described in this study, SNPs and lipids were injected within the aqueous and ethanolic phases respectively. The serpentine-shaped mixing channel of the reactor (Figure 1) was designed to enhance the mixing process between ethanol and water. This mixing enhancement was attributed to the increase in the residence time of substances within the device, compared to a straight channel counterpart, and to the onset of advection-dominated mass transport due to the formation of secondary flows across the channel's cross-section (also referred to as Dean flows) [35]. The encapsulation of SNPs was expected to occur simultaneously with the formation of lipid vesicles, and SNPs were anticipated to mainly localise within the aqueous core of the liposome given their affinity to polar solvents.

The flow settings and formulations employed in continuous-flow liposome production in this study were comparable to those often used in other studies reporting on liposome production by solvent-exchange mechanism. However, modifications to the production conditions had to be applied in some cases, to meet specific requirements of the techniques used for particle characterisation in the present study. For example, for the evaluation of SNP encapsulation using TEM analysis, the volumetric flow rates and concentration of lipids and SNPs were increased to allow observation of a greater number of vesicles encapsulating SNPs. Concerning the analysis of the sample's zeta potential, the formulation conditions were modified considering the effect of pH, final particle size, and compatibility between different lipid types [35].

3.2 Image-based determination of SNPs encapsulation

Figure 2 shows representative TEM images of empty liposomes and SNPs, providing a characterization of their geometry and morphology. The synthesis of empty liposomes was performed using a formulation of PC:Chol (14.2:11.8 mM) at TFR of 1 ml/min and FRR of 10 (Batch code #1 in Table 1).

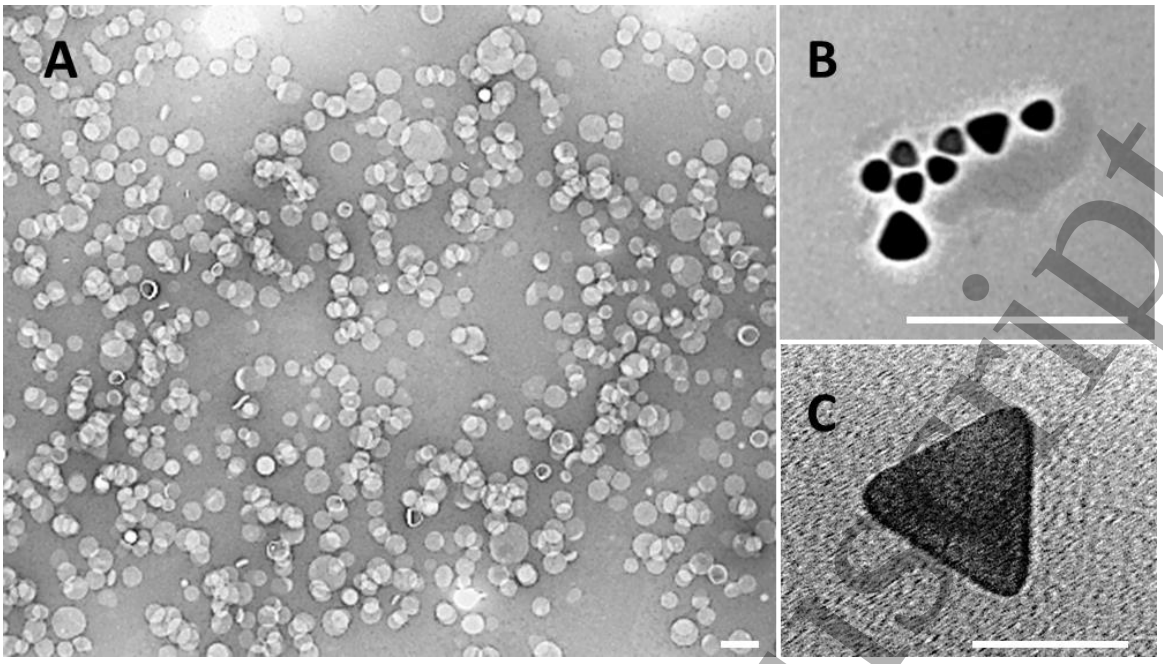

Figure 2. TEM images of (A) empty liposomes, and (B) and (C) SNPs. Scale bars: 200 nm, 200 nm, and 50 nm, respectively. Liposomes comprised of PC:Chol (11.2:4.8 mM) and were produced using the millifluidic reactor, at total flow rate (TFR) of 1 ml/min and flow rate ratio (FRR, flow of aqueous phase/ethanolic lipid solution) of 10.

As can be seen in Figure 2A, liposomes were largely spherical in shape and were effectively dispersed overall, having an average size between about 70 nm and 130 nm as calculated by MATLAB R2020 (using the 'imfindcircle' function). Some level of liposome overlapping can be appreciated from the image, and could likely be attributed to the sample preparation process and the high liposome concentration. Concerning the sample of SNPs, typical triangular-shaped nanoplates were observed. In some cases, SNPs presented rounded corners when the size decreased (Figure 2B); an individual SNP with an edge length of ~55 nm can be seen in Figure 2C. The size of SNPs, determined as the edge length of nanoplates, was measured manually using ImageJ to be between 20 – 50 nm.

Figure 3 illustrates some representative TEM images of Lipo/SNP samples, comprising PC:Chol (28:12 mM) and synthesized at TFR of 5 ml/min and FRR of 10 (Batch code #2 in Table 1).

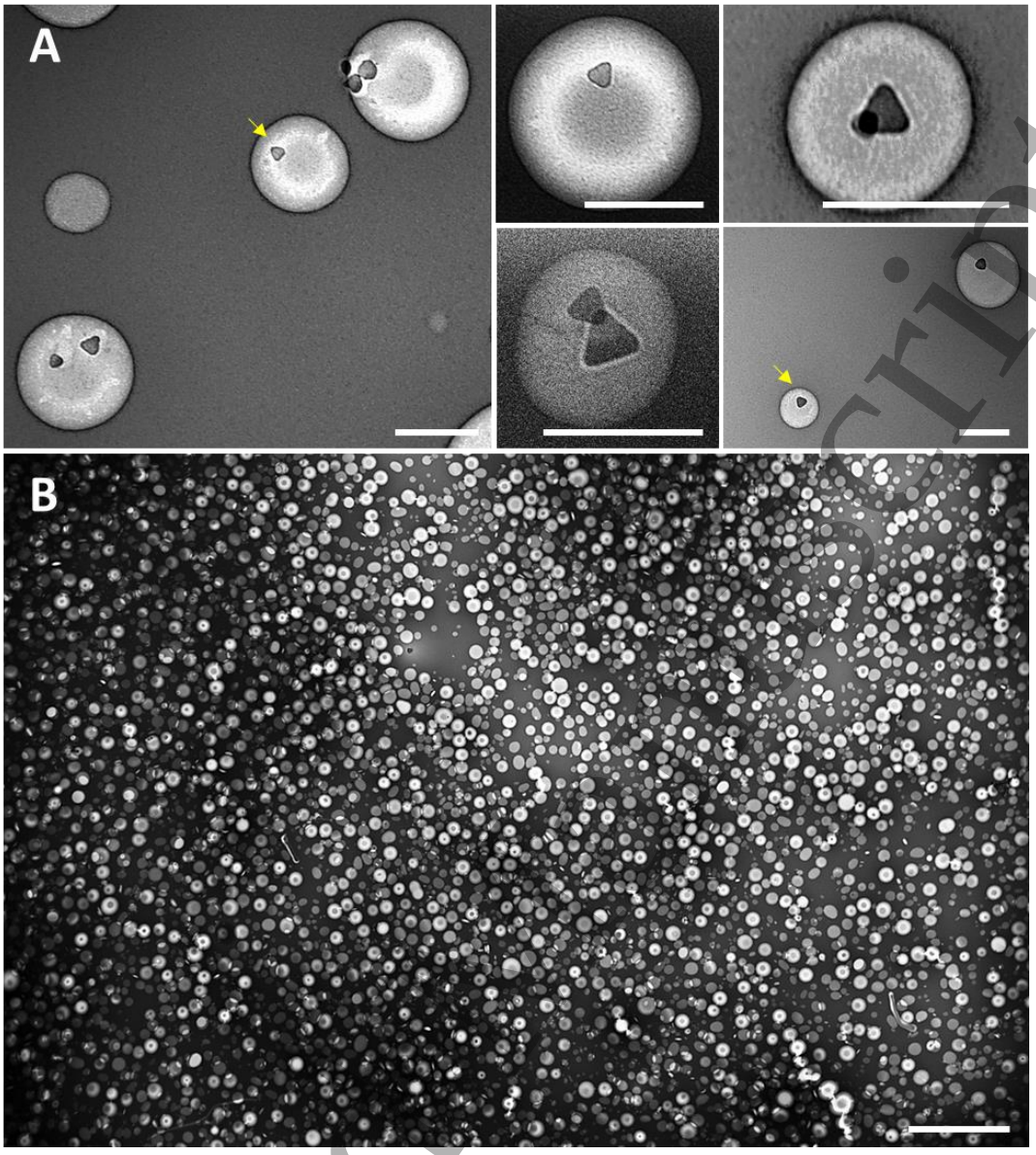

Figure 3. TEM images of Lipo/SNP samples comprising PC:Chol (28:12 mM), produced using the millifluidic reactor at total flow rate (TFR) of 5 ml/min and flow rate ratio (FRR) of 10. Images were selected from the same sample. (A) Bright circular structures and dark structures (mainly triangular-shaped) represent liposomes and SNPs, respectively. The yellow arrows point toward some of the SNPs that were encapsulated within, or attached to, liposomes. (B) Raw TEM image of Lipo/SNP sample, corresponding to the selected area used for the calculation of encapsulation efficiency. Scale bars: 200 nm, applied to all images in (A) and 2000 nm in (B), respectively.

The TEM images in Figure 3A clearly show liposomes as circular structures as well as triangular-shaped SNPs in the Lipo/SNP samples that were characterized just after production, without performing any particle separation or filtration process. Some of the observed liposomes had a single SNP associated, likely encapsulated inside the liposome core. Some SNPs instead appeared to be located outside the liposome circular structure, and were believed to be attached to the liposome outer membrane surface rather than being encapsulated within the aqueous core. However, the images provided insufficient spatial information about the SNPs location, i.e. whether they are positioned on the surface, within the bilayer, or inside the liposome core. Nonetheless, images confirmed that SNPs were interacting with the liposomes in many cases. The *EE*% was estimated by manually counting free SNPs and encapsulated/associated

SNPs, and a value of 77.48% was determined based on the image shown in Figure 3B on a representative selected region of the grid (see Figure S-1 in supplementary section for a larger section of the grid). It is important to note that the Lipo/SNP sample was negatively stained for the imaging procedure, which may have led to underestimating the number of free/unencapsulated SNPs, especially in areas where the concentration of stain was greater and may have masked some of the SNPs. Overall, the TEM technique was found to be an acceptable method to visualise and quantify the encapsulation of SNPs in liposomes. However, the associated staining procedure and its two-dimensional nature were found to be the main limitations associated with this imaging method.

To address these limitations, an additional experiment was performed in order to further assess the encapsulation of SNPs in liposomes. Lipo/SNP samples were prepared and embedded in resin, which was then sliced into thin sections (thickness of 800-900 Å) for imaging (Figure 4). The Lipo/SNP sample formulation comprised PC (100 mM) and was produced at TFR of 1 ml/min and FRR of 25 (Batch code #3 in Table 1).

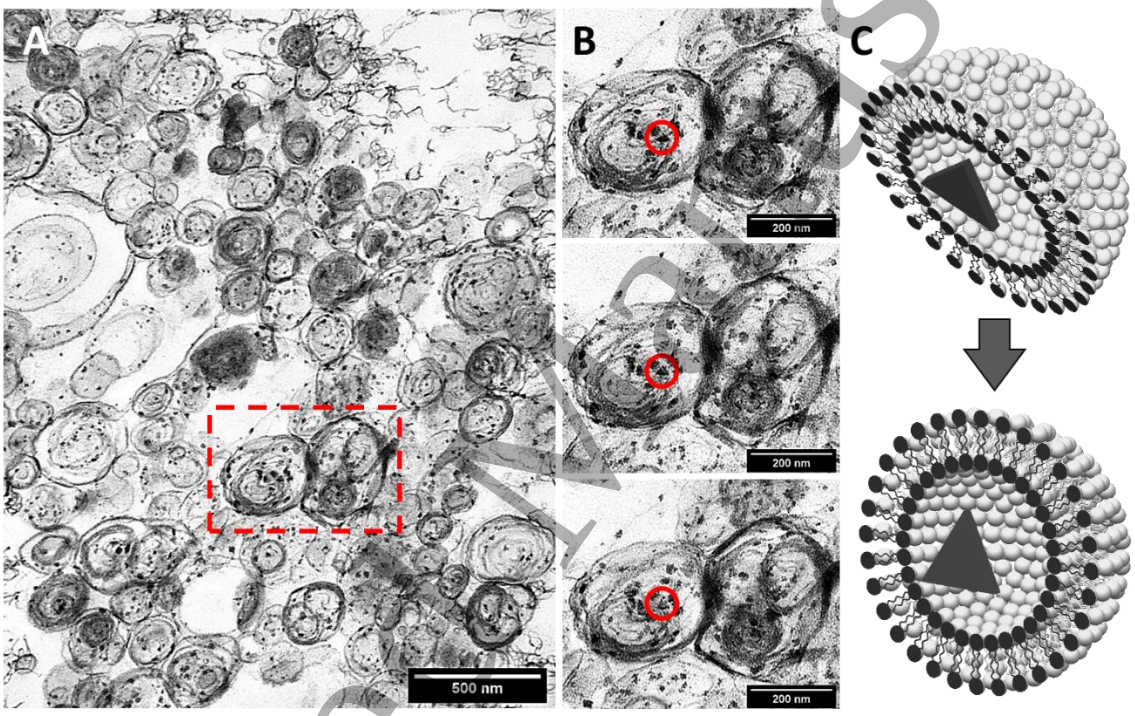

Figure 4. (A) TEM image of Lipo/SNP sample embedded in resin. (B) Images show a zoomed in view of the TEM image of a Lipo/SNP sample. The images (from top to bottom in B) were collected by tilting the holder of the TEM machine (changing the angle of the holder from +30° to -30°). (C) The illustration shows how the triangular nanoparticles (SNPs) encapsulated in liposomes are viewed when the angle of the imaging plane is tilted. Lipo/SNP sample comprised of PC (100 mM) and was produced using the millifluidic reactor, at total flow rate (TFR) of 1 ml/min and flow rate ratio (FRR) of 25.

As shown in Figure 4A, vesicular structures were observed along with darker material located mostly inside the liposomes or in their proximity. The darker particles were thought to be mostly AgNPs, and a few residual particulate material resulting from the sample preparation process. For confirmation, a selected region was specifically analysed by processing the images acquired at different angles (varying between +30° and -30°), as shown in Figure 4B (see Section S.2 in the supplementary material section for the animated image). It was evidently demonstrated in these images that an SNP was encapsulated within the liposome. In particular, in the bottom image of Figure 4B, a top view of the triangular structure becomes apparent, which is consistent with the schematics shown in Figure 4C.

Although it could be argued that not all of the dark material in the image corresponded to AgNPs, the encapsulation of SNPs in liposomes appeared to be highly efficient. Also, it is important to note that the exact location of SNPs (i.e., either within the aqueous core or within/associated with the liposome shell) could not be verified from these images. The technique was however found to be effective in demonstrating the association of SNPs with liposomes. Future research may include detailed characterization of Lipo/SNPs prepared with various concentrations of SNPs or liposomes, which could potentially lead to further our understanding of the encapsulation process.

3.3 Analysis of encapsulation by dimensional and zeta potential measurements

The encapsulation of SNPs in liposomes was also characterized in terms of particle size distribution and zeta potential (i.e. particle surface charge), using a DLS apparatus. The liposome sample formulation was PC:Chol (11.2:4.8 mM) and was produced at TFR of 1 ml/min and FRR of 10 (Batch code #1 in Table 1).

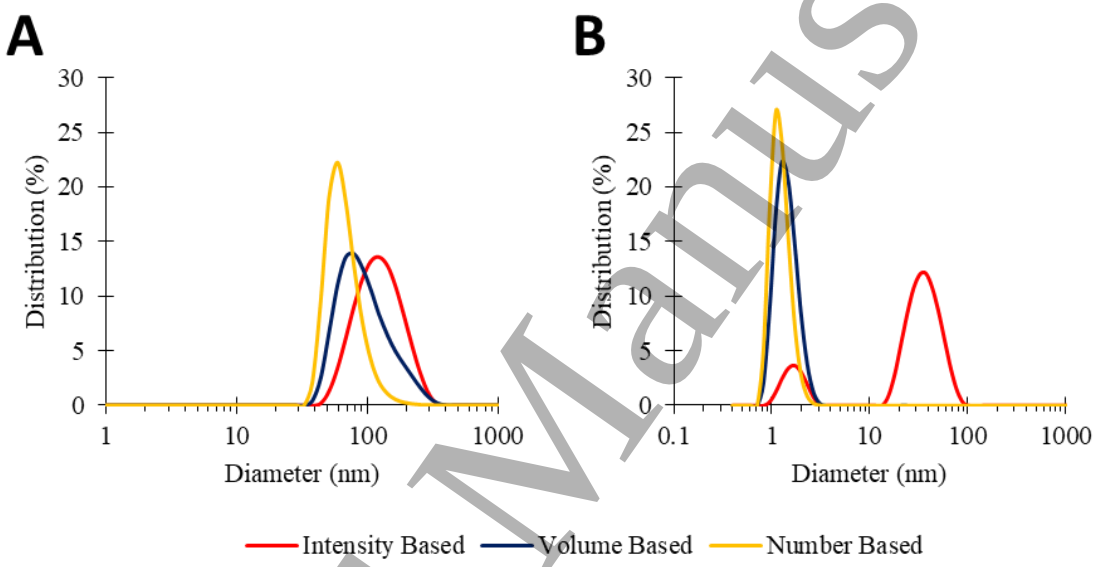

Figure 5. Size distribution of (A) liposomes comprising PC:Chol (11.2:4.8 mM) and produced using the millifluidic reactor, at total flow rate (TFR) of 1 ml/min and flow rate ratio (FRR) of 10, and (B) size distribution of SNPs. The solid lines represent the intensity- (red), volume- (blue), and number-based (yellow) size distributions.

Figure 5 shows the size distribution plots of empty liposomes and SNPs (measured by DLS), including intensity-, volume- and number-based distributions. The interpretation of the size distributions was primarily made by considering the intensity-based distributions (as detailed in Section 2.5.1), which were generally understood to be more reliable than the number- and volume-based distributions [39,40]. For all populations, the number and intensity-based distributions showed the lowest and highest peak values, respectively, which is consistent with the literature [39,40]. Based on intensity-based distributions, the average size of the neutral liposomes was approximately 120 nm (Figure 5A). In addition, the bell-shaped single peak indicated that the dispersions were relatively homogeneous, without significant interparticle aggregation. Furthermore, the dispersity index of liposomes was reasonably low, being 0.146 ± 0.022 for neutral liposomes, indicating a low dispersity of the particle hydrodynamic radius [43].

However, the size distribution profile of AgNPs exhibited two distinct peaks at approximately 2 nm and 35 nm, respectively (Figure 5B). Based on previously reported TEM images of SNPs (Figure 2B and C), these were expected to have an average size between 15 and 50 nm. Therefore, the peak at around 35

nm likely corresponded to SNPs, while the peak at ~2 nm was possibly related to the smaller spherical AgNPs.

It should be noted that the reported size of nanoparticles obtained from DLS was slightly different from the size measured by TEM. This was likely due to the assumptions made by the DLS algorithm when determining the hydrodynamic radius of the nanoparticles [39]. Also, it was observed during measurements that SNPs presented slightly different size peaks over multiple runs (where each measurement consisted of 11 runs); this could be related to possible nanoparticle aggregation, which could have caused an overestimate of nanoparticle size. Nevertheless, the combination of these techniques provided complementary information on nanoparticle geometry, in particular, for characterizing groups of particles with different shape and size.

Figure 6 illustrates the size distributions and zeta potential values of empty liposomes, SNPs, and Lipo/SNPs. For liposomal dispersions, the zeta potential is an indicator of the surface charge of the nanoparticle, and can provide information about the association of different types of nanoparticles with each other in colloidal dispersions [45]. The liposomal dispersions evaluated consisted of PC (16 mM) and were produced at TFR of 1 ml/min and FRR of 10 (Batch code #4 in Table 1).

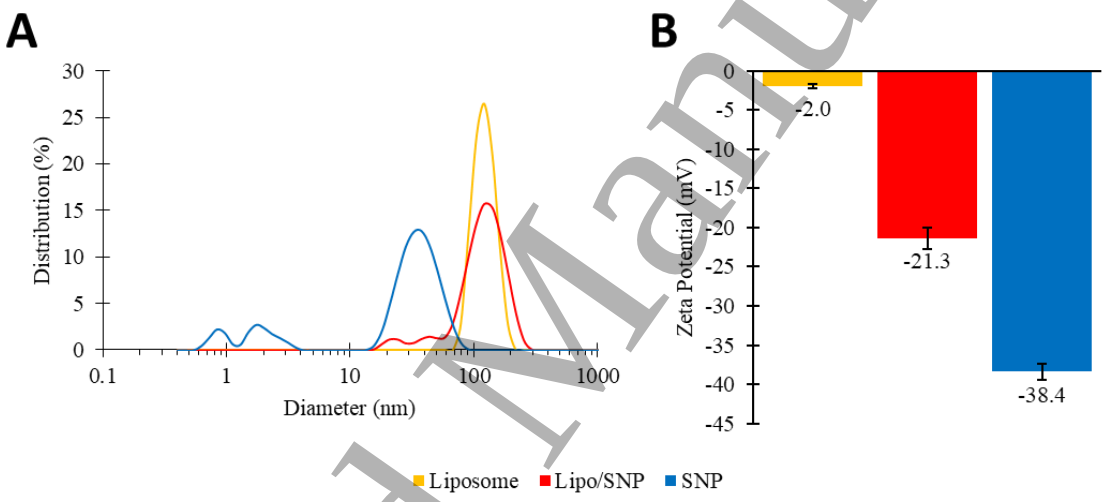

Figure 6. (A) Size distribution plots and (B) zeta potential values of liposome (yellow), Lipo/SNP (red), and SNP (blue) samples. Liposomal samples comprised of PC (16 mM) and were produced using the millifluidic reactor, at total flow rate (TFR) of 1 ml/min and flow rate ratio (FRR) of 10.

The size distribution profiles showed that SNPs and liposomes had peak sizes of 40 nm and 130 nm, respectively, corresponding to approximately their average size (Figure 6A). Lipo/SNPs showed an increased peak size of ~150 nm, which is likely indicative of the encapsulation of SNPs in liposomes.

Figure 6B shows that the average zeta potential values of liposomes and SNPs were -2 mV and -38.4 mV, respectively. The model lipid (i.e., PC) employed for the production of liposomes is neutral, resulting in the formation of liposomes having substantially no net surface charge [45]. However, when the lipids were mixed with SNPs in the flow reactor, the resulting Lipo/SNPs dispersion had a zeta potential value of -21.3 mV, suggesting that the SNPs charge (-38.4 mV) was partially "masked" by the liposomes as a result of encapsulation. Additionally, the zeta potential profile showed only a single peak indicating that there was only one type of nanoparticle in the dispersion (data not shown). Based on these findings, it can be further confirmed that SNP encapsulation was achieved to some extent. Interestingly, these findings further demonstrate the use of zeta potential as an indicator of the interaction between different colloidal systems, consistently with previous research [46,47].

4. Conclusion

Liposomes encapsulating SNPs (Lipo/SNPs) were synthesised using a continuous-flow millimetre-scale reactor (or millireactor), having a serpentine-like architecture in the flow channel to enhance mixing. The synthesis process was optimised by varying liposome composition and also the operating fluidic parameters, including flow rate ratio and total flow rate, to achieve formation of liposomes with low size dispersity and high *EE*%. The obtained Lipo/SNPs were characterised with different techniques including DLS, zeta potential measurements, and TEM imaging. Lipo/SNPs were found to have an average size of ~150 nm (size dispersity < 0.3), which is compatible with medicinal liposomal formulations. TEM image analysis revealed the average *EE*% to be 77.48%, with mostly single SNPs encapsulated in liposome envelopes. By using a multiangle (+30^{o} to -30^{o}) TEM imaging approach, quasi-3D images were obtained and further confirmed the encapsulation of nanoparticles within liposomes, providing a simple and effective method for locating nanoparticles within encapsulating structures. For a more definite quantification of *EE%* and precise spatial characterisation of SNPs encapsulation, further studies are required employing different characterisation techniques or procedures that can provide separation of unentrapped material or allow 3D imaging (such as Cryo-TEM). Furthermore, the photothermal performance of SNPs encapsulated in liposomes remains to be characterised for application in stimuli-mediated drug delivery.

Author Contributions: Liposome and Lipo/SNP production, F.Y.; SNP production H.K. and D.A.C., TEM and DLS characterization F.Y., design of the flow reactor, D.C.; fabrication of the flow reactor, A.M.; writing—review and editing F.Y., D.C., X.Z.; supervision, D.C., X.Z. All authors have read and agreed to the published version of the manuscript.

Funding: Turkish Ministry of National Education.

Acknowledgements: This paper was produced from the PhD research of F.Y. at Faculty of Engineering and Physical Sciences, University of Southampton. F.Y. thanks the Turkish Ministry of National Education for funding of his PhD scholarship.

Conflicts of Interest: The authors declare no conflict of interest.

References

[1] Calderón-Jiménez B, Johnson M E, Montoro Bustos A R, Murphy K E, Winchester M R and Vega Baudrit J R 2017 Silver nanoparticles: Technological advances, societal impacts, and metrological challenges *Frontiers in chemistry* **5** 6

[2] Keat C L, Aziz A, Eid A M and Elmarzugi N A 2015 Biosynthesis of nanoparticles and silver nanoparticles *Bioresources and Bioprocessing* **2** 1–11

[3] Mulvaney S P, Musick M D, Keating C D and Natan M J 2003 Glass-coated, analyte-tagged nanoparticles: a new tagging system based on detection with surface-enhanced Raman scattering *Langmuir* **19** 4784–90

[4] Doering W E, Piotti M E, Natan M J and Freeman R G 2007 SERS as a foundation for nanoscale, optically detected biological labels *Advanced Materials* **19** 3100–8

[5] Aygün A, Gülbağça F, Nas M S, Alma M H, Çalımlı M H, Ustaoglu B, Altunoglu Y C, Baloğlu M C, Cellat K and Şen F 2020 Biological synthesis of silver nanoparticles using Rheum ribes and evaluation of their anticarcinogenic and antimicrobial potential: A novel approach in phytonanotechnology *Journal of pharmaceutical and biomedical analysis* **179** 113012

[6] Zhang X-F, Liu Z-G, Shen W and Gurunathan S 2016 Silver nanoparticles: synthesis, characterization, properties, applications, and therapeutic approaches *International journal of molecular sciences* **17** 1534

[7] Das C A, Kumar V G, Dhas T S, Karthick V, Govindaraju K, Joselin J M and Baalamurugan J 2020 Antibacterial activity of silver nanoparticles (biosynthesis): A short review on recent advances *Biocatalysis and Agricultural Biotechnology* **27** 101593

[8] Noguez C 2007 Surface plasmons on metal nanoparticles: the influence of shape and physical environment *The Journal of Physical Chemistry C* **111** 3806–19

[9] Millstone J E, Hurst S J, Métraux G S, Cutler J I and Mirkin C A 2009 Colloidal gold and silver triangular nanoprisms *Small* **5** 646–64

[10] Xue B, Wang D, Zuo J, Kong X, Zhang Y, Liu X, Tu L, Chang Y, Li C and Wu F 2015 Towards high quality triangular silver nanoprisms: improved synthesis, six-tip based hot spots and ultra-high local surface plasmon resonance sensitivity *Nanoscale* **7** 8048–57

[11] Xu X, Wang Y, Wang H, Su H, Mao X, Jiang L, Liu M, Sun D and Hou S 2016 Synthesis of triangular silver nanoprisms and studies on the interactions with human serum albumin *Journal of molecular liquids* **220** 14–20

[12] Panzarasa G 2015 Just what is it that makes silver nanoprisms so different, so appealing? *Journal of Chemical Education* **92** 1918–23

[13] Gao C, Lu Z, Liu Y, Zhang Q, Chi M, Cheng Q and Yin Y 2012 Highly stable silver nanoplates for surface plasmon resonance biosensing *Angewandte Chemie International Edition* **51** 5629–33

[14] Boca S C, Potara M, Gabudean A-M, Juhem A, Baldeck P L and Astilean S 2011 Chitosan-coated triangular silver nanoparticles as a novel class of biocompatible, highly effective photothermal transducers for in vitro cancer cell therapy *Cancer Letters* **311** 131–40

[15] Ciou S-H, Cao Y-W, Huang H-C, Su D-Y and Huang C-L 2009 SERS enhancement factors studies of silver nanoprism and spherical nanoparticle colloids in the presence of bromide ions *The Journal of Physical Chemistry C* **113** 9520–5

[16] Kulkarni A P, Noone K M, Munechika K, Guyer S R and Ginger D S 2010 Plasmon-enhanced charge carrier generation in organic photovoltaic films using silver nanoprisms *Nano letters* **10** 1501–5

[17] Xue Y, Zhang S, Huang Y, Zhang T, Liu X, Hu Y, Zhang Z and Tang M 2012 Acute toxic effects and gender-related biokinetics of silver nanoparticles following an intravenous injection in mice *Journal of Applied Toxicology* **32** 890–9

[18] Lee S H and Jun B-H 2019 Silver Nanoparticles: Synthesis and Application for Nanomedicine *Int J Mol Sci* **20** 865

[19] Seong M and Lee D G 2017 Silver Nanoparticles Against Salmonella enterica Serotype Typhimurium: Role of Inner Membrane Dysfunction *Curr Microbiol* **74** 661–70

[20] Long Y-M, Hu L-G, Yan X-T, Zhao X-C, Zhou Q-F, Cai Y and Jiang G-B 2017 Surface ligand controls silver ion release of nanosilver and its antibacterial activity against Escherichia coli *Int J Nanomedicine* **12** 3193–206

[21] Foldbjerg R, Irving E S, Hayashi Y, Sutherland D S, Thorsen K, Autrup H and Beer C 2012 Global gene expression profiling of human lung epithelial cells after exposure to nanosilver *Toxicol Sci* **130** 145–57

[22] Lin J, Huang Z, Wu H, Zhou W, Jin P, Wei P, Zhang Y, Zheng F, Zhang J, Xu J, Hu Y, Wang Y, Li Y, Gu N and Wen L 2014 Inhibition of autophagy enhances the anticancer activity of silver nanoparticles *Autophagy* **10** 2006–20

[23] Sriram M I, Kalishwaralal K, Barathmanikanth S and Gurunathani S 2012 Size-based cytotoxicity of silver nanoparticles in bovine retinal endothelial cells *Nanoscience Methods* **1** 56–77

[24] Stoehr L C, Gonzalez E, Stampfl A, Casals E, Duschl A, Puntes V and Oostingh G J 2011 Shape matters: effects of silver nanospheres and wires on human alveolar epithelial cells *Particle and fibre toxicology* **8** 1–15

[25] Yusuf A, Brophy A, Gorey B and Casey A 2018 Liposomal encapsulation of silver nanoparticles enhances cytotoxicity and causes induction of reactive oxygen species-independent apoptosis *Journal of Applied Toxicology* **38** 616–27

[26] Yusuf A and Casey A 2020 Evaluation of silver nanoparticle encapsulation in DPPC-based liposome by different methods for enhanced cytotoxicity *International Journal of Polymeric Materials and Polymeric Biomaterials* **69** 860–71

[27] Barenholz Y (Chezy) 2012 Doxil® — The first FDA-approved nano-drug: Lessons learned *Journal of Controlled Release* **160** 117–34

[28] Hofheinz R-D, Gnad-Vogt S U, Beyer U and Hochhaus A 2005 Liposomal encapsulated anti-cancer drugs *Anti-cancer drugs* **16** 691–707

[29] Gürsoy A, Kut E and Özkırımlı S 2004 Co-encapsulation of isoniazid and rifampicin in liposomes and characterization of liposomes by derivative spectroscopy *International journal of pharmaceutics* **271** 115–23

[30] Akbarzadeh A, Rezaei-Sadabady R, Davaran S, Joo S W, Zarghami N, Hanifehpour Y, Samiei M, Kouhi M and Nejati-Koshki K 2013 Liposome: classification, preparation, and applications *Nanoscale research letters* **8** 1–9

[31] Gabizon A, Dagan A, Goren D, Barenholz Y and Fuks Z 1982 Liposomes as in vivo carriers of adriamycin: reduced cardiac uptake and preserved antitumor activity in mice *Cancer research* **42** 4734–9

[32] Malam Y, Loizidou M and Seifalian A M 2009 Liposomes and nanoparticles: nanosized vehicles for drug delivery in cancer *Trends in pharmacological sciences* **30** 592–9

[33] Lv S, Jing R, Liu X, Shi H, Shi Y, Wang X, Zhao X, Cao K and Lv Z 2021 One-Step Microfluidic Fabrication of Multi-Responsive Liposomes for Targeted Delivery of Doxorubicin Synergism with Photothermal Effect *Int J Nanomedicine* **16** 7759–72

[34] Leung A K K, Tam Y Y C, Chen S, Hafez I M and Cullis P R 2015 Microfluidic Mixing: A General Method for Encapsulating Macromolecules in Lipid Nanoparticle Systems *J. Phys. Chem. B* **119** 8698–706

[35] Yanar F, Mosayyebi A, Nastruzzi C, Carugo D and Zhang X 2020 Continuous-Flow Production of Liposomes with a Millireactor under Varying Fluidic Conditions *Pharmaceutics* **12** 1001

[36] Cristaldi D A, Yanar F, Mosayyebi A, García-Manrique P, Stulz E, Carugo D and Zhang X 2018 Easy-to-perform and cost-effective fabrication of continuous-flow reactors and their application for nanomaterials synthesis *New biotechnology* **47** 1–7

[37] Carugo D, Lee J Y, Pora A, Browning R J, Capretto L, Nastruzzi C and Stride E 2016 Facile and cost-effective production of microscale PDMS architectures using a combined micromilling-replica moulding (μ Mi-REM) technique *Biomedical microdevices* **18** 1–10

[38] Hills E E, Abraham M H, Hersey A and Bevan C D 2011 Diffusion coefficients in ethanol and in water at 298 K: Linear free energy relationships *Fluid Phase Equilibria* **303** 45–55

[39] Stetefeld J, McKenna S A and Patel T R 2016 Dynamic light scattering: a practical guide and applications in biomedical sciences *Biophys Rev* **8** 409–27

[40] Iego S 2012 A guide to dynamic light scattering measurement and analysis

[41] Danaei M, Dehghankhold M, Ataei S, Hasanzadeh Davarani F, Javanmard R, Dokhani A, Khorasani S and Mozafari M R 2018 Impact of particle size and polydispersity index on the clinical applications of lipidic nanocarrier systems *Pharmaceutics* **10** 57

[42] Jahn A, Stavis S M, Hong J S, Vreeland W N, DeVoe D L and Gaitan M 2010 Microfluidic mixing and the formation of nanoscale lipid vesicles *ACS nano* **4** 2077–87

[43] Jahn A, Vreeland W N, DeVoe D L, Locascio L E and Gaitan M 2007 Microfluidic directed formation of liposomes of controlled size *Langmuir* **23** 6289–93

[44] Kimura N, Maeki M, Sato Y, Note Y, Ishida A, Tani H, Harashima H and Tokeshi M 2018 Development of the iLiNP device: fine tuning the lipid nanoparticle size within 10 nm for drug delivery *ACS omega* **3** 5044–51

[45] Clogston J D and Patri A K 2011 Zeta potential measurement *Characterization of nanoparticles intended for drug delivery* 63–70

[46] Honary S and Zahir F 2013 Effect of zeta potential on the properties of nano-drug delivery systems-a review (Part 1) *Tropical journal of pharmaceutical research* **12** 255–64

[47] Vogel R, Pal A K, Jambhrunkar S, Patel P, Thakur S S, Reátegui E, Parekh H S, Saá P, Stassinopoulos A and Broom M F 2017 High-resolution single particle zeta potential characterisation of biological nanoparticles using tunable resistive pulse sensing *Scientific reports* **7** 17479